Earthquakes and Structures, Vol. 3, No. 3-4 (2012) 341-363

DOI: http://dx.doi.org/10.12989/eas.2012.3.3.341

Criteria for processing response-spectrum-compatible seismic accelerations simulated via spectral representation

A. Zerva*[1], H. Morikawa[2] and S. Sawada[3]

[1]Department of Civil, Architectural and Environmental Engineering, Drexel University, 3141 Chestnut Street, Philadelphia, PA 19104, USA
[2]Department of Built Environment, Tokyo Institute of Technology, 4259-G3-7 Nagatsuta, Midori-ku, Yokohama 226-8502, Japan
[3]Disaster Prevention Research Institute, Kyoto University, Gokasho, Uji, Kyoto, 611-0011, Japan

(Received July 11, 2011, Revised December 11, 2011, Accepted April 10, 2012)

Abstract. The spectral representation method is a quick and versatile tool for the generation of spatially variable, response-spectrum-compatible simulations to be used in the nonlinear seismic response evaluation of extended structures, such as bridges. However, just as recorded data, these simulated accelerations require processing, but, unlike recorded data, the reasons for their processing are purely numerical. Hence, the criteria for the processing of acceleration simulations need to be tied to the effect of processing on the structural response. This paper presents a framework for processing acceleration simulations that is based on seismological approaches for processing recorded data, but establishes the corner frequency of the high-pass filter by minimizing the effect of processing on the response of the structural system, for the response evaluation of which the ground motions were generated. The proposed two-step criterion selects the filter corner frequency by considering both the dynamic and the pseudo-static response of the systems. First, it ensures that the linear/nonlinear dynamic structural response induced by the processed simulations captures the characteristics of the system's dynamic response caused by the unprocessed simulations, the frequency content of which is fully compatible with the target response spectrum. Second, it examines the adequacy of the selected estimate for the filter corner frequency by evaluating the pseudo-static response of the system subjected to spatially variable excitations. It is noted that the first step of this two-fold criterion suffices for the establishment of the corner frequency for the processing of acceleration time series generated at a single ground-surface location to be used in the seismic response evaluation of, e.g. a building structure. Furthermore, the concept also applies for the processing of acceleration time series generated by means of any approach that does not provide physical considerations for the selection of the corner frequency of the high-pass filter.

Keywords: acceleration simulations; velocity and displacement time series; spatial variation; response spectrum; spectral representation; processing; corner frequency; high-pass filter; nonlinear seismic response; bridges

1. Introduction

Lifeline systems, e.g. bridges, are subjected to spatially variable ground motions during earthquakes. This effect has started being incorporated in seismic design provisions, as, e.g. the New York City

*Corresponding author, Professor, E-mail: aspa@drexel.edu

DOT Seismic Design Criteria (NYCDOT 1998) and the EUROCODE 8, Part 2: Bridges (CEN 2005). In the absence of recorded data at distances appropriate for the supports of bridges, these seismic codes either provide the designers with conditionally simulated spatially variable ground motions that can be used with minor modifications (NYCDOT 1998), or recommend, in a rigorous approach, the simulation of spatially variable excitations generated via versions of the spectral representation method (CEN 2005). Conditional simulations are based on a recorded accelerogram, which may be scaled to a target response spectrum. To preserve the non-stationarity of the recorded motions in the processes of conditional simulation, the accelerogram is segmented, each segment is conditionally simulated based on a spatial coherency model, and the segments are pieced together (e.g. Liao and Zerva 2006). On the other hand, simulated spatially variable ground motions are artificially generated to comply with the spatial coherency model and power or response spectral densities. The vast majority of studies considering the effect of the spatial variation of the seismic ground motions on the response of bridges utilize versions of the spectral representation method (e.g. Burdette *et al*. 2008a, 2008b, Lou and Zerva 2005, Lupoi *et al*. 2005, Monti *et al*. 1996, Saxena *et al*. 2000, Shinozuka *et al*. 2001, Tzanetos *et al*. 2000).

At first glance, processing of the simulated acceleration time series generated via the spectral representation method does not appear to be an issue, as they are derived by purely numerical means. Indeed, the need for processing may not become apparent to the user if they utilize acceleration time histories in a, e.g. Monte Carlo analysis of a building structure. It suffices that the simulations conform to the prescribed target characteristics. The situation reverses, however, when spatially variable ground motions are generated for the seismic response of a lifeline system, as, e.g. a bridge. Numerical (finite element) codes permitting spatially variable motions as excitations at the structure's supports require, generally, displacement time series as input motions. The reason for this requirement is that spatially variable excitations induce the pseudo-static response of lifelines, which is controlled by the ground displacements. However, displacement time series obtained through direct double integration of simulated accelerations do not exhibit realistic waveforms, because the acceleration time series can contain large, numerically generated amplitude variability in the low frequency range. In this case, the need for processing becomes apparent. However, there are no guidelines or agreed-upon approaches to be followed in the processing of such simulated acceleration time series, and, generally, the type of processing utilized is not disclosed.

Criteria developed by the seismological community for the selection of the corner frequency of the high-pass filter in the processing of recorded data cannot be directly applied to simulated motions. The reason is that there are physical causes underlying the existence of the excess low-frequency components in the records, and processing approaches for recorded data rely on physical considerations, as, e.g. signal-to-noise ratio. This information establishes the characteristics of the appropriate high-pass filter that eliminates the low-frequency components in the records. On the other hand, the low-frequency components in simulated accelerations are numerically generated. Hence, the establishment of a cut-off frequency, below which the lower frequency components in the simulations can be reliably eliminated, is not a straight-forward task. This paper sets the bases for the establishment of a framework for processing spatially variable acceleration time series generated as response-spectrum compatible by means of the spectral representation method or any other simulation scheme that does not provide physical considerations for the selection of the corner frequency of the high-pass filter (e.g. Moustafa *et al*. 2010, Spanos *et al*. 2009). In the absence of physical criteria directing the elimination of lower frequency components in the simulations, the approach allows the selection of the appropriate corner frequency of the processing filter to be guided by its effect on the structural response, for the evaluation of which the ground motions are generated.

2. Simulations generated via spectral representation

The most commonly used approach for the generation of spatially variable, non-stationary and response-spectrum compatible simulations is the spectral representation method (Deodatis 1996, Hao *et al.* 1989). Consider that spatially variable ground motions are to be generated at M locations on the ground surface as non-stationary random processes obeying a coherency model and power spectral densities that are compatible with prescribed spectra. Following Deodatis (1996), the motions are initially generated as stationary based on the cross spectral density matrix, $\mathbf{S}^0(\omega_k)$, the elements of which are given by

$$[\mathbf{S}^0(\omega_k)]_{lm} = \gamma(\xi_{lm}, \omega_k)\sqrt{S_{ll}(\omega_k)S_{mm}(\omega_k)} \tag{1}$$

where $\gamma(\xi_{lm},\omega_k)$ is the spatial variability term, incorporating both loss of coherency and apparent propagation of the seismic excitations; ξ_{lm} indicates the separation distance between two locations l and m (e.g. two bridge supports); ω_k is the discrete frequency in rad/s; and $S_{ll}(\omega_k)$ and $S_{mm}(\omega_k)$ are the power spectral densities at the two locations. Cholesky decomposition is then applied to the cross spectral density matrix of Eq. (1), i.e., $\boldsymbol{S}^0(\omega_k) = \boldsymbol{C}_k^T\boldsymbol{C}_k$, with the superscript T indicating transpose. Spatially variable acceleration time series are then simulated in sequence according to the expression (Deodatis 1996)

$$a_l(t) = 2\sqrt{\Delta\omega}\sum_{m=1}^{l}\sum_{k=1}^{K}|C_{lm}(\omega_k)|\mathbf{cos}(\omega_k t + \theta_{lm}(\omega_k) + \phi_{mk}); \quad l = 1,...,M \tag{2}$$

in which $|C_{lm}(\omega_k)|$ is the absolute value of element lm of $\mathbf{C}_k$; $\theta_{lm}(\omega_k)$ is its phase, reflecting the apparent propagation effect on the simulated motions; and ϕ_{mk} are random phase angles uniformly distributed between $[0, 2\pi)$. The utilization of the Fast Fourier Transform in Eq. 1 (Shinozuka 1974, Zerva 1992a) dramatically reduces the computational time for the simulations, and makes the approach a quick and versatile tool for the generation of vast numbers of artificial spatially variable ground motions.

Eq. 2 generates the time series as stationary and compatible with the coherency model and the power spectral densities. Non-stationarity is imposed in the simulations through their multiplication by an intensity modulating function. This process introduces low-frequency components in the time series (Safak and Boore 1988). Furthermore, for the motions to become response-spectrum compatible, their power spectral densities are initially given an assumed functional form, and the simulations are then iteratively modified at each location to match the target response spectrum. In the iteration process, either the Fourier amplitudes of the motions are adjusted to the target response spectrum as in Eq. 3(a) below (Hao *et al.* 1989), or their power spectrum is upgraded to the target response spectrum as in Eq. 3(b) (Deodatis 1996)

$$A_l^{i+1}(\omega_k) = A_l^i(\omega_k)\frac{RS_l(\omega_k)}{RS_{sl}^i(\omega_k)} \tag{3a}$$

$$S_{ll}^{i+1}(\omega_k) = S_{ll}^i(\omega_k)\left[\frac{RS_l(\omega_k)}{RS_{sl}^i(\omega_k)}\right]^2 \tag{3b}$$

In the above equations, $A_l^i(\omega_k)$ and $A_l^{i+1}(\omega_k)$ are the Fourier amplitudes of the simulations at the l-th station for the i-th and (i+1)-th iterations, respectively; $S_{ll}^i(\omega_k)$ and $S_{ll}^{i+1}(\omega_k)$ the corresponding power spectral densities; $RS_l(\omega_k)$ is the target response spectrum at station l; and $RS_{sl}^i(\omega_k)$ is the response spectrum of the simulated motion at the station for the i-th iteration. The new estimates for the amplitudes, obtained either directly from Eq. 3(a) or through the power spectrum from Eq. 3(b), are then used in the simulation of the random field, and the process is repeated until satisfactory agreement between the simulated and the target response spectra is achieved. With the aforementioned process, seldom will the response spectrum of each simulation match perfectly the target response spectrum. Some numerically artificial components will be introduced in the iterative process over the entire frequency range of the simulations, in addition to the low-frequency components introduced through the intensity modulation of the time series. These components will affect the acceleration simulations, but, their low-frequency part will affect significantly the velocity and displacement time series integrated from the accelerations. This is illustrated in the following example that applies the aforementioned process for the generation of simulations at a single station l, and will be further utilized herein for the establishment of criteria for the processing of response-spectrum compatible acceleration simulations based on the spectral representation method.

For the realizations of the random process at a single station, Eq. (2) reduces to

$$a_l(t) = 2\sum_{k=1}^{K}[S_{ll}^0(\omega_k)\Delta\omega]^{1/2}\mathbf{cos}(\omega_k t + \phi_k) \tag{4}$$

which is the spectral representation form introduced by Rice (1944), and applied to simulations of random processes and fields by Shinozuka (1971). Fig. 1(a) presents an example acceleration simulation compatible to the ASCE 7-10 (ASCE 2010) response spectrum scaled to 0.5 g; the parameters of the spectrum in this illustration are $S_{DS} = 0.5$, $S_{D1} = 0.2$ and $T_L = 8$ s. The intensity modulating function utilized is of the form (Amin and Ang 1968)

$$I(t) = \begin{cases} (t/t_1)^2 & 0 \le t \le t_1 \\ 1 & t_1 \le t \le t_2 \\ \mathbf{exp}[-b(t-t_2)] & t \ge t_2 \end{cases} \tag{5}$$

with parameters $t_1 = 2$ s, $t_2 = 9$ s, $b = 0.4$/s, and the total duration of the simulation being 30 s. The simulation was iteratively modified to match the target spectrum by means of Eq. 3(a) (Hao *et al.* 1989). Short taper functions were introduced at the beginning and the end of the acceleration simulation to bring its values to zero. Part (b) of Fig. 1 illustrates the velocity time series resulting from the integration of the acceleration simulation, part (c) the displacement waveform obtained through double integration of the acceleration, and part (d) the comparison of the response spectrum

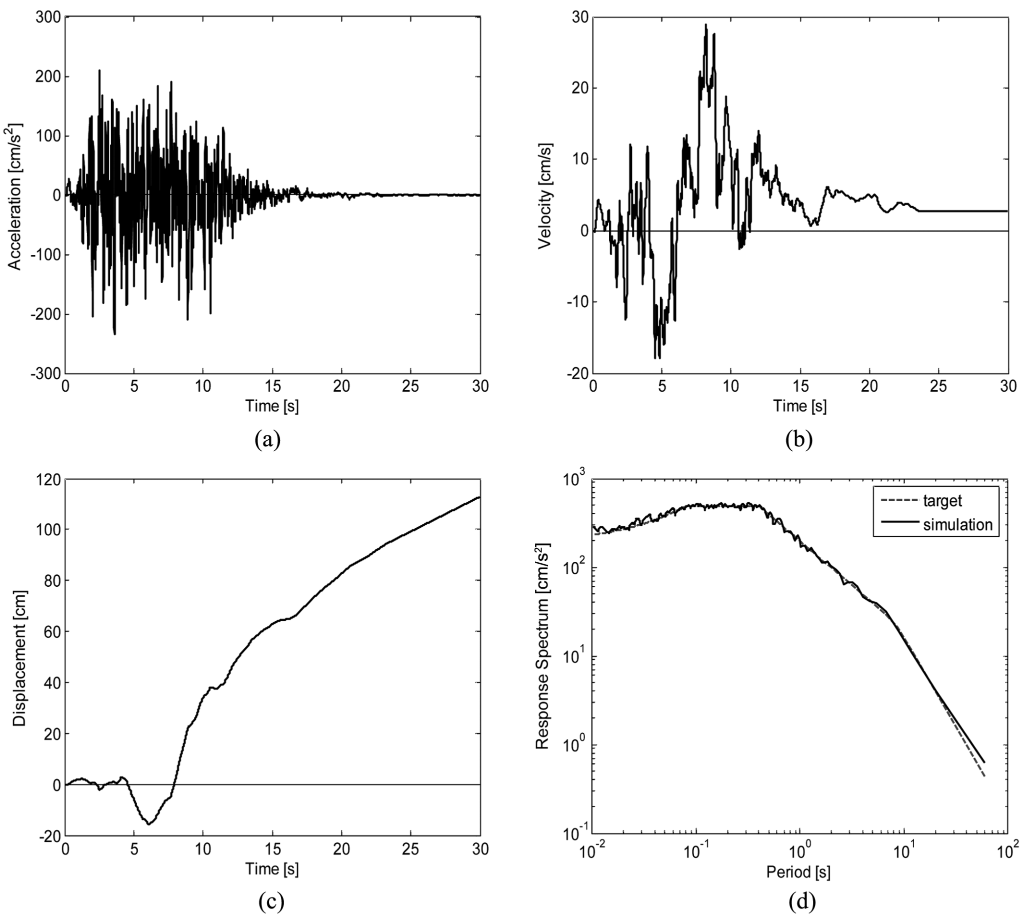

Fig. 1 Unprocessed acceleration, velocity and displacement simulations in parts (a), (b) and (c), respectively, and comparison of the response spectrum of the simulation with the target response spectrum in part (d)

of the simulation with the target response spectrum. It can be seen from the figure that the acceleration time series has a reasonable form (Fig. 1(a)), that the response spectrum of the simulation is in reasonable agreement with the target response spectrum (Fig. 1(d)), but that the velocity time series tends to constant values at the end of the record (Fig. 1(b)), and that the value of the displacement keeps increasing with increasing time (Fig. 1(c)). The unrealistic form of the velocities and displacements in Figs. 1(b) and (c) are caused by the artificial generation of the low-frequency components in the simulations. Hence, the processing of simulations, just like the processing of recorded data, is a necessity, but the reason for processing these simulations is purely numerical.

3. Processing of seismic data

A variety of methods have been proposed in the literature for processing earthquake records (e.g. Boore and Bommer 2005, Boore *et al.* 2002, Converse and Brady 1991, Trifunac 1971). The simplest processing scheme (Boore 2011) is to apply a high-pass filter to the acceleration time series. The following choices are available for the selection of the characteristics of the high-pass filter: (1) filter type; (2) filter order; (3) filter corner frequency and (4) causal or acausal filtering.

Boore and Bommer (2005) indicated that data processing is not sensitive to the choice of a particular high-pass filter type, but, instead, depends highly on the value of the corner frequency of the filter. Following the processing approaches used by the California Strong Motion Instrumentation Program, the US Geological Survey and the Pacific Earthquake Engineering Research Center, this study utilizes the Butterworth filter. The modulus of the frequency transfer function of the Butterworth filter is given by

$$|H_n(f)| = \left[\frac{(f/f_c)^{2n}}{1+(f/f_c)^{2n}}\right]^{1/2} \tag{6}$$

where n indicates the order of the filter and f_c its corner frequency. Fig. 2(a) presents the modulus of the response of a high-pass (low-cut) Butterworth filter for various orders (n = 2, 3, 4, 6 and 8) and a corner frequency of f_c = 0.09 Hz, i.e., frequencies lower than 0.09 Hz are, at least, partially removed. For the lower orders of the filter, frequencies higher than the corner frequency are also partially removed. On the other hand, as the filter order increases, the cut-off of the lower frequencies becomes more abrupt. Following Boore *et al.* (2002), a 4-th order Butterworth high-pass filter is utilized.

The selection of the appropriate corner frequency, f_c, for the processing of simulated acceleration time series is essentially, the focus of this work. In the processing of earthquake ground motion, records, the corner frequency is determined from the signal-to-noise ratio, so that most of the background noise is removed from the signal. If such information is not available, the corner frequency, f_c, can be estimated, e.g. from the value of the frequency for which the Fourier amplitude

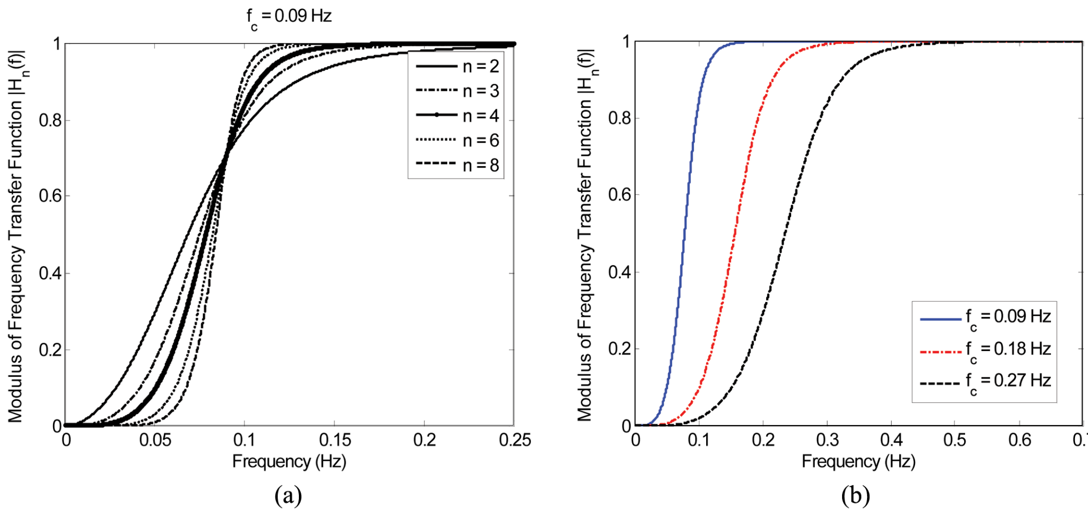

Fig. 2 The variation of the modulus of the frequency transfer function of a high-pass Butterworth filter with filter order and corner frequency: part (a) for a fixed corner frequency f_c = 0.09 Hz and orders n = 2, 3, 4, 6 and 8, and part (b) for a fixed order n = 4 and corner frequencies f_c = 0.09 Hz, 0.18 Hz and 0.27 Hz

spectrum of the record no longer tends to zero at low frequencies (Zaré and Bard 2002), since the theoretical shape of the far-field Fourier amplitude spectrum decreases as ω^2 at low frequencies, or determined iteratively, within a frequency range lower than the values of the frequencies obtained from theoretical Fourier amplitude spectra of the event, until the displacement time series exhibit realistic waveforms (Akkar and Bommer 2006). The situation in numerical simulations is, however, different, since there is no background noise involved in the process of simulation, but, as indicated earlier, the generated motions can be contaminated by, e.g. large low-frequency randomly simulated Fourier amplitudes. Liao and Zerva (2006) proposed a purely numerical criterion to evaluate the corner frequency of the selected filter in conditionally simulating spatially variable ground motions. The corner frequency value is selected such that most of the low-frequency components, whose corresponding periods are longer than the duration T of the simulated time histories, are removed. For example, if $|H_0|$ denotes the modulus of the transfer function of a continuous high-pass n-th order Butterworth filter corresponding to frequency $f_0 = 1/T$ (Eq. 6), the corner frequency can be evaluated as

$$f_c = \frac{1}{T}\left[\frac{1}{H_0^2} - 1\right]^{\frac{1}{2n}} \tag{7}$$

i.e., the corner frequency depends on the duration of the simulated time series and the filter amplitude threshold $|H_0|$ at $f_0 = 1/T$. Liao and Zerva (2006) also suggested that the amplitude threshold be selected as $|H_0| = 0.02$, which means that at least 98% of the low-frequency components with periods longer than the duration of the simulated time history are filtered out. Hence, if the simulated time series is 30 s long, as in the example illustration of Fig. 1, and a 4-th order Butterworth filter is utilized, then the corner frequency is determined as approximately 0.09 Hz (0.0886 Hz). In a sense, this selection criterion mimics the one used for seismic records by assuming that a small fraction of the simulated low-frequency components represents “noise” in the simulations. It is emphasized, however, that, whereas noise exists in recorded data, all components of the simulated motions are generated such that their response spectrum matches the target one (Fig. 1(d)). Three filter corner frequencies are selected for the subsequent evaluations. The first is 0.09 Hz as recommended by Liao and Zerva (2006). The second and third are 0.18 Hz and 0.27 Hz, i.e., two and three times the value of the first corner frequency. For these latter two values at least 99.88% and 99.98%, respectively, of the low-frequency components with periods longer than the duration of the simulated time history are filtered out. The modulus of the frequency transfer function of the Butterworth filter for the three selected corner frequencies is illustrated in Fig. 2(b). It can be seen from the figure that the higher the value of the corner frequency, the more significant the elimination of lower frequency components in the filtered time series.

Regarding the selection of causal vs. acausal filtering, acausal filtering is utilized in the subsequent analyses for the estimation of the corner frequency in the processing of the simulations. The reason is that the process of causal filtering causes phase distortions of the time series depending on the value of the corner frequency (Boore and Akkar 2003). On the other hand, acausal filtering is zero-phase and does not cause distortion of the waveforms. The zero-phase shift is achieved in the time domain by applying the filter one time from the beginning to the end of the record, and then another time by reversing the order and applying the filter from the end of the record to the beginning. It should be noted that, because acausal filtering filters the time series twice, the order of the Butterworth filter used in acausal filtering should be $n/2$, if n is the order of the Butterworth filter used in the corresponding causal filtering. Obviously, the use of acausal filtering has the advantage of not causing phase distortions in the time series. However, acausal filtering requires zero-padding at both ends, which results in longer time series. The reason that this zero-padding is required is that, to achieve zero-phase shifts, the filtering operation has to start before the beginning of the record in the forward filtering and, in the reverse process, after the end of the record. The zero-padding length depends on the value of the selected corner frequency and the order of the filter, as suggested in the empirical expression by Converse and Brady (1992)

$$t_{pad} = \frac{3n}{4f_c} \tag{8}$$

in which t_{pad} is the zero-padding length (in [s]) at both the beginning and the end of the time series to be processed by means of acausal filtering.

4. Effect of processing on simulated ground motions

The effect of the corner frequency of the acausal filtering operation on the generated accelerations, the integrated velocity and displacement time series, and the response spectra of the simulations is illustrated in Figs. 3-5. Specifically, Fig. 3 presents the effect of the processing procedure highlighted in Section 3 when the corner frequency is equal to 0.09 Hz, Fig. 4 the results when the corner frequency is 0.18 Hz, and Fig. 5 when the value of the corner frequency is 0.27 Hz. Part (a) of the figures presents the accelerations, part (b) the velocities, part (c) the displacements and part (d) the comparison of the response spectra resulting from the simulations with the target response spectrum. It is noted that the time scale in parts (a), (b) and (c) of Figs. 1 and 3-5 differs. The duration of the original time series in Fig. 1 is 30 s. Because of zero-padding, which is inversely proportional to the value of the corner frequency (Eq. 8), the duration of the processed simulations in Figs. 3, 4 and 5 is 63.33 s, 46.67 s and 41.11 s, respectively.

For consistency with Fig. 1(a), the same seed for the generation of the random phase angles (Eq. 4) was utilized in the simulation of the acceleration time series in Figs. 3(a), 4(a) and 5(a). As a consequence, the shape as well as the amplitude of the acceleration waveforms in parts (a) of Figs. 1 and 3-5 is fairly similar. This should be expected, as accelerations constitute the higher frequency component of the motions. On the other hand, very significant differences are observed in the comparison of the velocity and displacement time series in parts (b) and (c), respectively, of Figs. 1 and 3-5. Whereas the velocity waveforms in Fig. 1(b) tend to a constant value and the displacement time series in Fig. 1(c) keep increasing with time, both velocities and displacements in parts (b) and (c), respectively, of Figs. 3-5 tend to zero. This is a consequence of the high-pass filtering, and, also, the sufficiency of the zero-padding at the beginning and the end of the simulations in the acausal processing scheme. However, both the shape and the peak values of the velocities and displacements in parts (b) and (c) of Figs. 3-5 vary significantly. The peak values of the velocity waveforms reduce from 20.2 cm/s for f_c = 0.09 Hz (Fig. 3(b)) to 15.5 cm/s for f_c = 0.18 Hz (Fig. 4(b)) and 14.5 cm/s for f_c = 0.27 Hz (Fig. 5(b)). For the displacements, the peak values reduce from 12.5 cm for f_c = 0.09 Hz (Fig. 3(c)) to approximately 6 cm for f_c = 0.18 Hz (Fig. 4(c)) and 3.7 cm for f_c = 0.27 Hz (Fig. 5(c)). This should be expected as velocities are more affected by the low-frequency content of the motions than accelerations, and displacements are controlled by the low-frequency components.

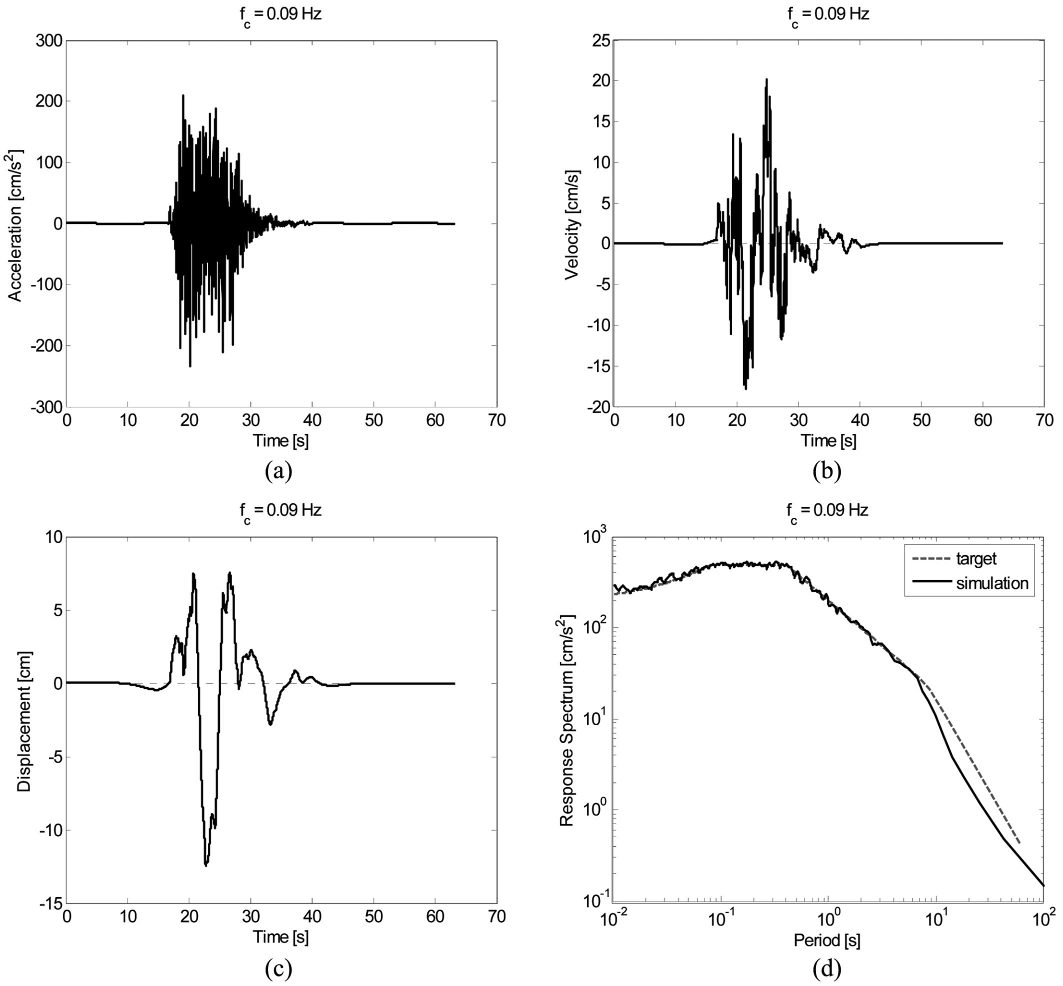

Fig. 3 Effect of acausal filtering with a corner frequency of f_c = 0.09 Hz on one acceleration simulation; processed acceleration, velocity and displacement time series are shown in parts (a), (b) and (c), respectively, and the comparison of the response spectrum of the simulation with the target response spectrum in part (d)

The comparison of the response spectrum of the unprocessed and processed acceleration time series in parts (d) of Figs. 1 and 3-5, respectively, clearly indicates that the match of the response spectrum of the unprocessed accelerations with the target response spectrum (Fig. 1(d)) is better than that of the processed time series (parts (d) of Figs. 3-5). The comparison of the response spectra of the processed simulations with the target values reflects the effect of the filtering operation. Whereas the response spectrum of the unprocessed acceleration time series in Fig. 1(d) slightly overestimates the target response spectrum at the short and long periods (high and low frequencies, respectively), the response spectra of the processed accelerations exhibit, as expected, the same behavior at the short periods (high frequencies), but underestimate the target response spectra at the long periods (low frequencies) depending on the value of the corner frequency of the processing filter. These differences will affect both the dynamic and the pseudo-static response of

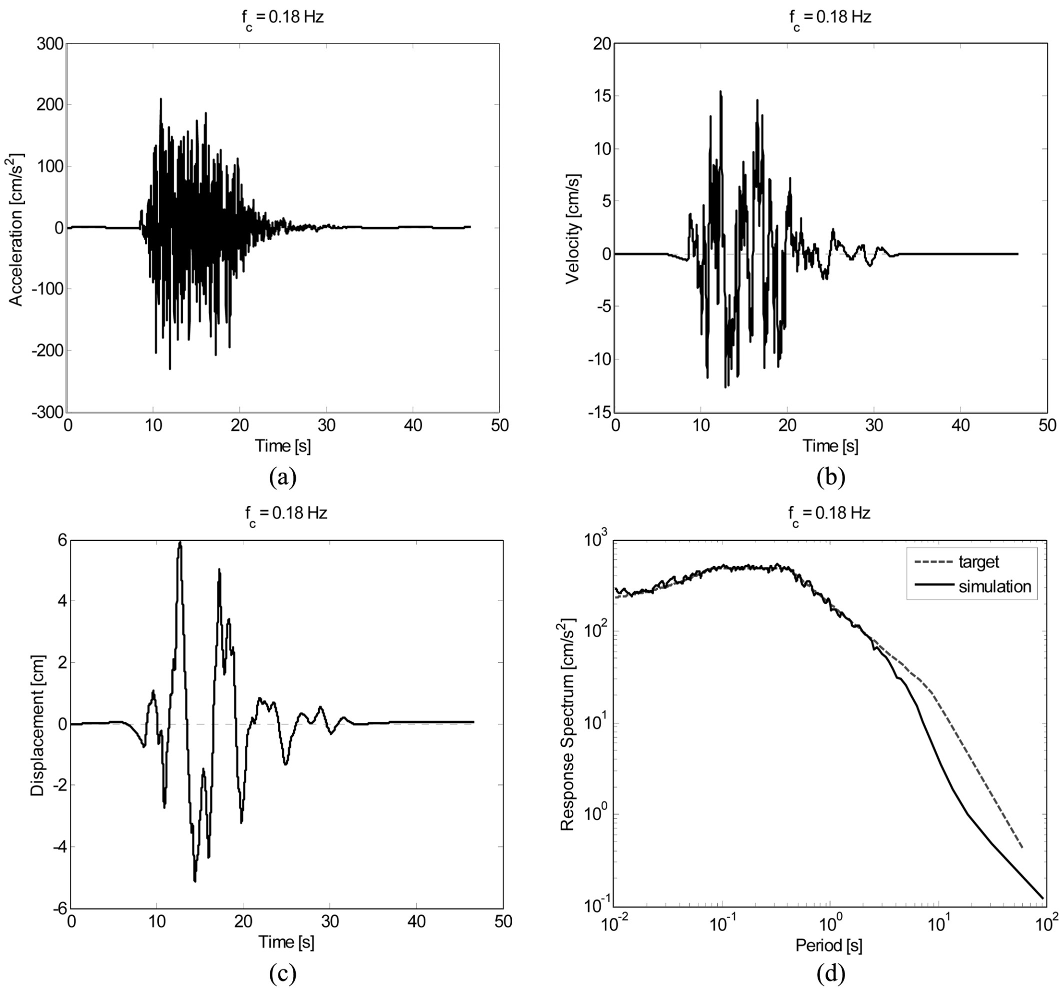

Fig. 4 Effect of acausal filtering with a corner frequency of $f_c = 0.18$ Hz on one acceleration simulation; processed acceleration, velocity and displacement time series are shown in parts (a), (b) and (c), respectively, and the comparison of the response spectrum of the simulation with the target response spectrum in part (d)

lifelines.

For each selected corner frequency ($f_c = 0.09$ Hz, 0.18 Hz and 0.27 Hz), 100 acceleration simulations were generated and processed. The statistics of the peak acceleration, velocity and displacement values of the processed simulations are presented in Fig. 6 in terms of cumulative distribution functions. Specifically, Fig. 6(a) presents the cumulative distribution function (CDF) of the peak acceleration for each processing case; for comparison purposes, the CDF of the peak value of 100 unprocessed acceleration simulations is also shown in the figure. As observed earlier in the comparison of parts (a) of Figs. 1 and 3-5, the acceleration waveforms are not significantly affected by the high-pass filtering process. Indeed, the variation of the peak values of the acceleration simulations, processed or unprocessed, is not statistically significant. Figs. 6(b) and (c) present the CDF of the peak ground velocity and peak ground displacement obtained for each processing case.

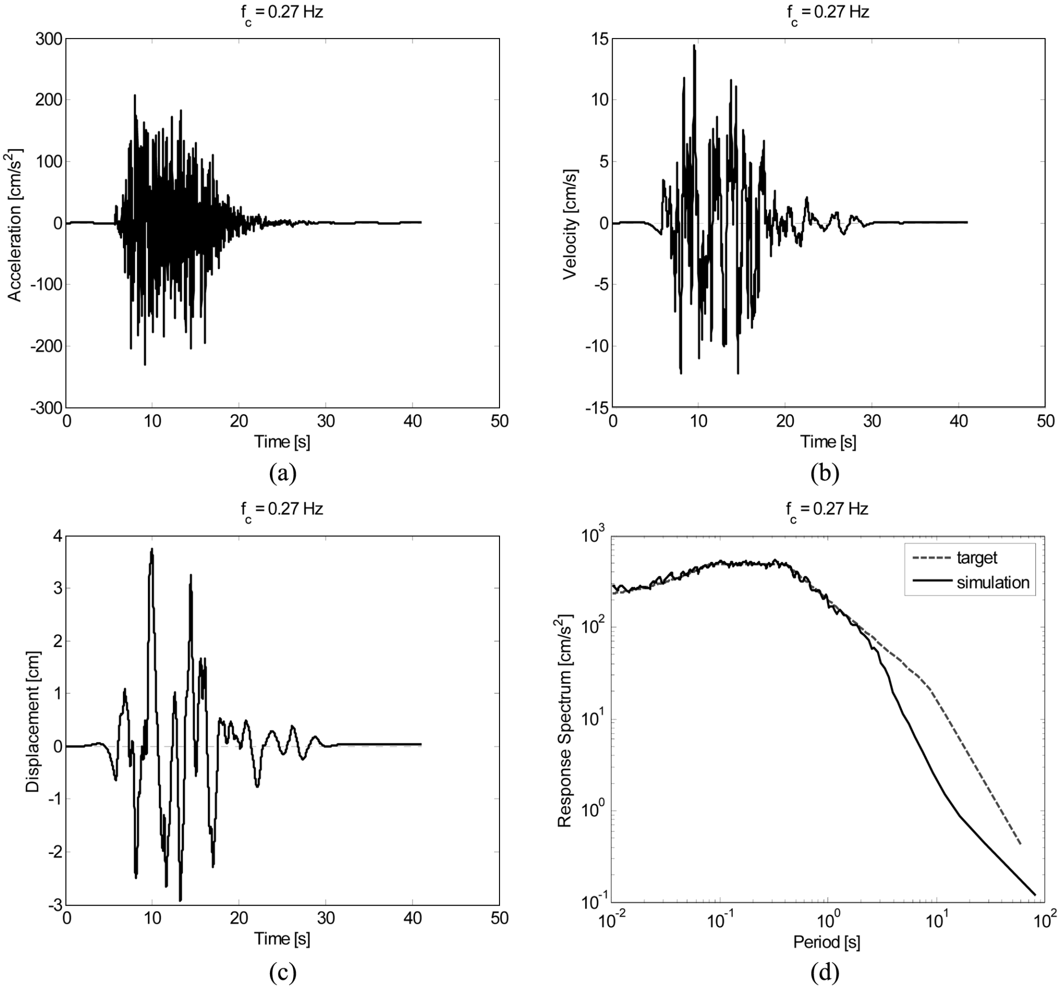

Fig. 5 Effect of acausal filtering with a corner frequency of $f_c = 0.27$ Hz on one acceleration simulation; processed acceleration, velocity and displacement time series are shown in parts (a), (b) and (c), respectively, and the comparison of the response spectrum of the simulation with the target response spectrum in part (d)

It is noted that the peak values of the ground velocities and displacements obtained by integrating the unprocessed acceleration simulations are not presented in these figures as they are meaningless (Figs. 1(b) and (c)). Figs. 6(b) and (c) clearly illustrate the effect of the value of the corner frequency on the statistics of the peak velocity and displacement: the higher the corner frequency, the lower the value of the peak velocity and displacement, and displacements are more affected than velocities. This ought to be expected, as displacements are controlled by the lower frequency components of the motions.

The comparisons of the waveforms in Figs. 1 and 3-5, and of the statistics of the peak values in Fig. 6, even though insightful, are inconclusive regarding the establishment of criteria for the selection of the appropriate value of the filter corner frequency that should be used in Monte Carlo simulations for the evaluation of the response of lifeline systems. In spite of their differences, the

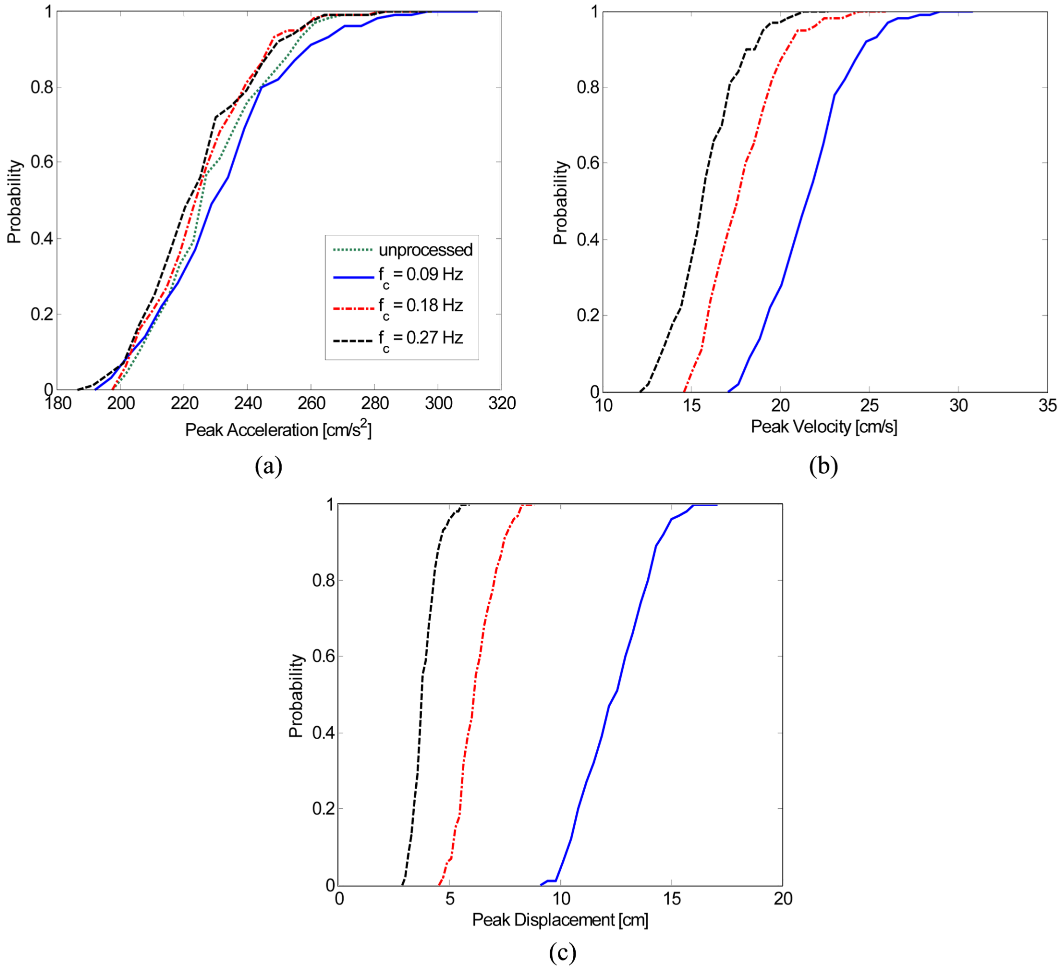

Fig. 6 Cumulative distribution functions of peak ground motion values obtained from 100 ground motion simulations processed with three filter corner frequencies, $f_c = 0.09$ Hz, 0.18 Hz and 0.27 Hz. Probability distributions for peak accelerations, velocities and displacements are shown in parts (a), (b) and (c) respectively; the probability distribution of unprocessed peak accelerations is also presented, for comparison purposes, in part (a)

waveforms in parts (a), (b) and (c) of Figs. 3-5 exhibit realistic behavior. Given that the cause for the existence of the low-frequency components in the simulations is purely numerical, the selection criterion for the appropriate corner frequency of the processing scheme needs to rely on the effect of processing on the structural response, which is elaborated upon in the following section.

5. Effect of simulation processing on the system response

The seismic response of lifelines subjected to spatially variable excitations is composed of the pseudo-static and dynamic response, whereas, when the systems are subjected to uniform excitations, only the dynamic response is excited. Clearly, the pseudo-static and dynamic responses are non-separable in a nonlinear analysis of the structures, as is the contribution of the individual dynamic modes. However, to establish generic criteria for the selection of the processing scheme for simulated spatially variable excitations, this approach separates the dynamic and pseudo-static response of the structures as illustrated in the following two subsections.

It should also be noted at this point that EUROCODE 8, Part 2: Bridges (CEN 2005), in its provisions for the approximate incorporation of the effect of the spatial variation of the seismic ground motions on the response of bridges, recommends that the dynamic and pseudo-static response of bridges be analyzed separately, and then combined via the square-root-of-sum-of-squares (SRSS) rule. The code suggests that an equivalent nonlinear analysis of the bridge be first performed considering a uniform excitation at all supports based on the worst-case scenario of support conditions. A pseudo-static analysis should then be conducted for "in-phase" displacements, that increase linearly from the first to the last support of the bridge, and completely "out-of-phase" displacements between subsequent supports. The worst pseudo-static response from the two scenarios should then be combined with the dynamic response via the SRSS rule. The recommendations in the following separate the dynamic and pseudo-static response of the structures only for the selection of the appropriate corner frequency of the high-pass filter.

5.1 Dynamic response

The following criterion is postulated for the selection of the filter corner frequency based on the dynamic response of the systems. Since the corner frequency affects mostly the frequency content of the excitations at low frequencies, it is realistic to assume that the structural mode mostly affected will be the fundamental mode. The most obvious and quick approach to visualize the effect of the high-pass filtering on the structural response would then be to compare the transfer function of the filter with that of a linear single-degree-of-freedom (SDOF) oscillator with natural frequency equal to the fundamental frequency of the lifeline system. The transfer functions of three linear SDOF oscillators with natural frequencies of f_n = 0.33 Hz, 1 Hz and 5 Hz are presented in Fig. 7. The natural frequency of 1 Hz was selected because the analysis of two short-span bridges taken from the seismic design examples 1 and 4 of the Federal Highway Administration (FHWA 1996a, b), a straight, two-span and a skewed, three-span bridge, indicated that that their fundamental frequencies were 1.19 Hz and 1.18 Hz, respectively (Lou 2006, Lou and Zerva 2005). Hence, this frequency reflects the fundamental frequency of, at least, these two highway bridges, and, even though it is higher than the filter corner frequencies utilized herein, it approaches their range. The higher frequency of 5 Hz was selected to illustrate the effect of the low-pass filtering on the dynamic response of systems with frequencies significantly higher than the corner frequency of the filter, as well as the effect of the corner frequency on the higher system modes. The low-valued natural frequency of 0.33 Hz was selected to reflect more flexible systems with natural frequencies in the vicinity of the corner frequencies of the filter. Damping in all cases was assumed to be 5% of critical. Superimposed in Fig. 7 are the transfer functions of the high-pass filters of Fig. 2(b) multiplied by a factor of two, so that their plots intersect the transfer functions of the SDOF oscillators above the plateau of unity. Fig. 7 indicates that, as expected, processing of the excitations would not affect the dynamic response of the stiffer systems (f_n = 5 Hz), as the dominant amplification range of the oscillator is far removed from the low frequencies filtered through processing. Similarly, for the oscillator with f_n = 1 Hz, the effect of processing with any of the considered corner frequencies does not appear to be significant, as the dominant amplification range

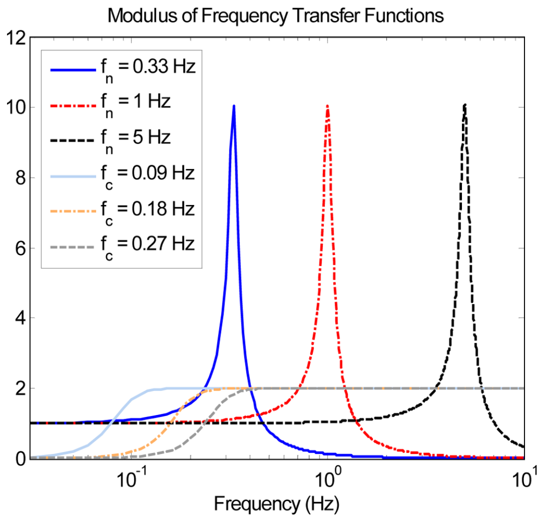

Fig. 7 The modulus of the frequency transfer functions of single-degree-of-freedom oscillators with natural frequencies of $f_n = 0.33$ Hz, 1 Hz and 5 Hz (pointed, darker lines in the plot), and twice the value of the modulus of the response of a high-pass Butterworth filter with corner frequencies $f_c = 0.09$ Hz, 0.18 Hz and 0.27 Hz (lighter lines in the plot)

of the oscillator occurs at higher frequencies than the ones filtered through processing. However, due to the relative proximity of the oscillator's frequency with the highest corner frequency considered, it may be speculated that the use of f_c = 0.27 Hz may not fully capture the response. For the flexible system ($f_n = 0.33$ Hz), it is evident from Fig. 7 that the corner frequency of f_c = 0.27 Hz would eliminate excitation frequencies necessary to capture the structural response. The corner frequency of $f_c = 0.18$ Hz also appears to affect the flexible system's response, as it reaches its constant level when the system's transfer function has started increasing. On the other hand, it may be speculated that the filter with f_c = 0.09 Hz is appropriate, as the eliminated frequencies are below the dominant amplification range of the oscillator. However, as for the case of the oscillator with $f_n = 1$ Hz and the filter with $f_c = 0.27$ Hz, it may be argued again that the lowest corner frequency is in relative proximity to the natural frequency of the more flexible system, and its use may still eliminate components of the excitation that affect the dynamic response.

Clearly, the comparisons in Fig. 7 are informative and indicative. However, the uncertainty regarding the selection of the filter corner frequencies for the lower natural frequency SDOF oscillators ($f_n = 0.33$ Hz and 1 Hz) cannot be resolved unless a more elaborate evaluation is performed. Furthermore, simulations are generally generated for the nonlinear response of the structural systems, which may be "softer" than their corresponding linear ones, and the seismic response is affected not only by the characteristics of the structure, but also, those of the seismic excitation. Therefore, it is proposed herein that a single-support, SDOF system with natural frequency equal to the fundamental frequency of the lifeline and similar nonlinear characteristics be subjected to processed and unprocessed simulations, and the filter corner frequency be selected such that the dynamic response caused by the processed simulations fully captures the dynamic response induced by the unprocessed ones. As an illustration of this quantitative criterion for the selection for the filter corner frequency, the sensitivity of the response of a nonlinear SDOF oscillator subjected to simulated time series processed with the various corner frequencies utilized herein is presented next.

The nonlinear behavior of the system is described by the Bouc-Wen model (Wen 1980). Consider a single-degree-of-freedom (SDOF) system being excited by the ground acceleration $a_g(t)$ at its support. The dynamic equilibrium equation of the system in terms of its relative response, $u(t)$, is

$$M\ddot{u}(t) + F(u, \dot{u}) = -Ma_g(t) \tag{9}$$

where M is the mass, $F(u, \dot{u})$ the total spring force, and overdot and double overdot indicate relative velocity and acceleration, respectively. According to the Bouc-Wen model (Wen 1980), the force $F(u, \dot{u})$ in Eq. 9 is given by the following expression

$$F(u, \dot{u}) = C\dot{u} + rKu + (1-r)Kz(u, \dot{u}) \tag{10}$$

where C indicates damping, K stiffness, r the ratio of post-yield to pre-yield stiffness, and $z(u, \dot{u})$ the total restoring force, modeled by the differential equation (Wen 1980)

$$\dot{z}(u, \dot{u}) = A\dot{u} - \alpha|\dot{u}||z(u, \dot{u})|^{\eta-1}z(u, \dot{u}) + \beta\dot{u}|z(u, \dot{u})|^{\eta} \tag{11}$$

In Eqs. 10 and 11, the parameters K, r and A control the initial stiffness; A, α, β and η the yield level; α and β the hysteresis shape; and η controls the sharpness of yield (Wen 1980). A softening hysteretic behavior with $\alpha + \beta > 0$ and $\alpha - \beta > 0$ (Wong *et al.* 1994) is selected herein for the nonlinear modeling of the SDOF oscillator. Fig. 8 illustrates the cyclic hysteretic behavior of the system for $r = 0.5$, $A = 1$, $\eta = 1$, $\alpha = 0.2$ and $\beta = 0.8$ in terms of the relation between the relative displacement and the hysteretic restoring force $z(u, \dot{u})$. The aforementioned parameters for the Bouc-Wen model along with the three previously selected natural frequencies ($f_n = 0.33$ Hz, 1 Hz and 5 Hz) are utilized in the sensitivity analysis of the response of SDOF oscillators to the value of the high-pass filter corner frequency. Damping for all cases is, again, assumed to be 5% of critical.

Each structural system is then subjected to four sets of 100 simulations. The first set includes unprocessed accelerations and serves as the anchor to which the results for the processed simulations

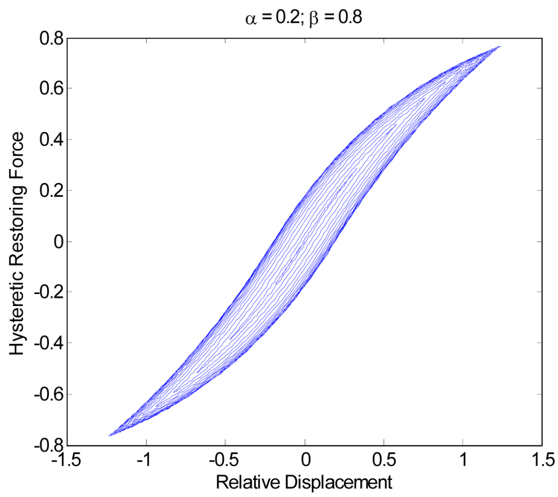

Fig. 8 Hysteretic softening behavior ($\alpha + \beta > 0$; $\alpha - \beta > 0$) of the Bouc-Wen model

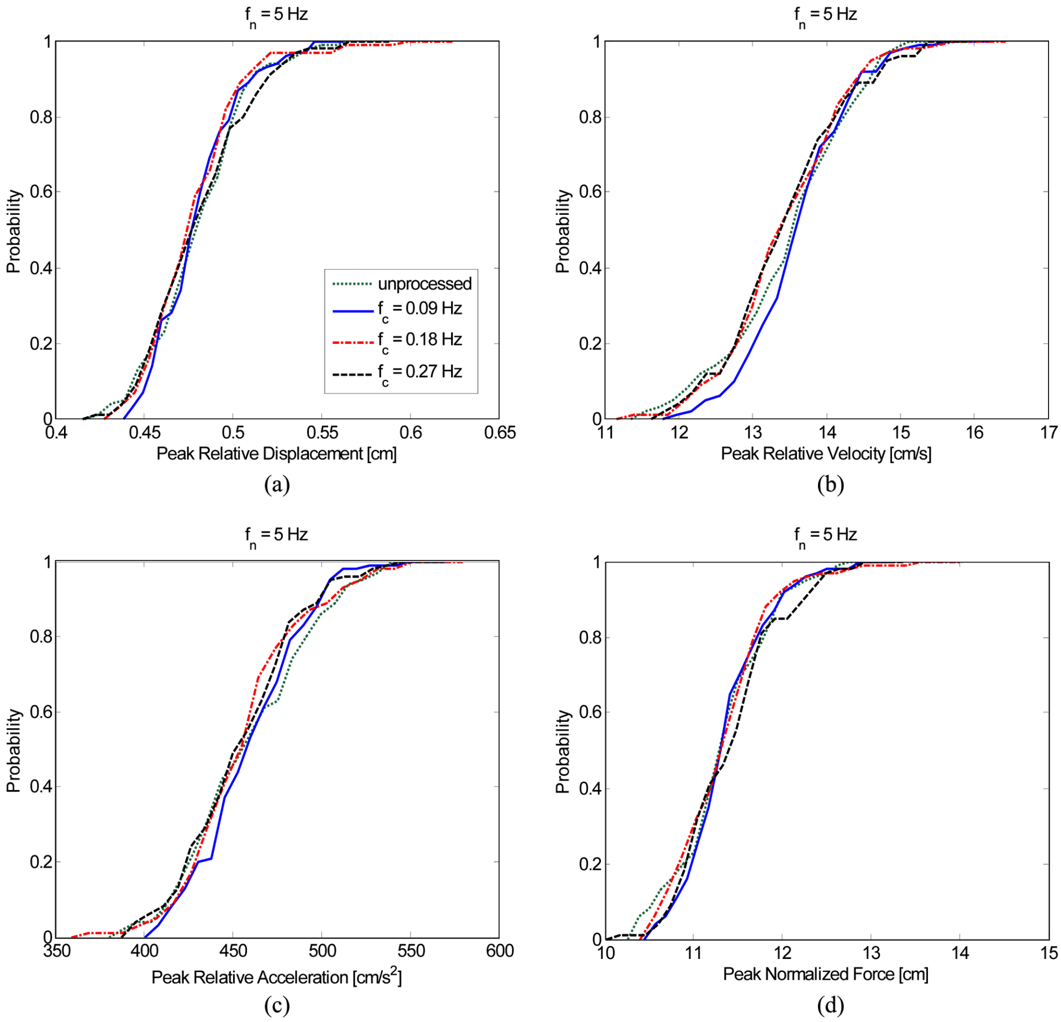

Fig. 9 Cumulative distribution functions of the peak response of a nonlinear single-degree-of-freedom oscillator with natural frequency $f_n = 5$ Hz subjected to sets of 100 ground motion simulations processed with three filter corner frequencies, $f_c = 0.09$ Hz, 0.18 Hz and 0.27 Hz; the oscillator's peak response subjected to a set of 100 unprocessed acceleration simulations is also shown in the figures. Part (a) presents the probability distribution of the oscillator's peak relative displacement, part (b) its peak relative velocity, part (c) its peak relative acceleration and part (d) the peak total spring force normalized with the system's stiffness

are compared. It is noted that this set would be the ideal one from all simulation sets, as it fully conforms to the response spectrum (Fig. 1(d)), but leads to unrealistic velocities and displacements (Figs. 1(b) and (c)). The three additional sets are comprised of simulations filtered with acausal filtering and corner frequencies of $f_c = 0.09$ Hz, 0.18 Hz and 0.27 Hz. The results of the dynamic response evaluation of the nonlinear oscillator with natural frequencies of $f_n = 5$ Hz, 1 Hz and 0.33 Hz are presented in Figs. 9, 10 and 11, respectively. Part (a) of the figures illustrates the statistics of the system's peak relative displacement, part (b) those of the peak relative velocity, part (c) those of the peak relative acceleration and part (d) the peak total spring force normalized with respect to the

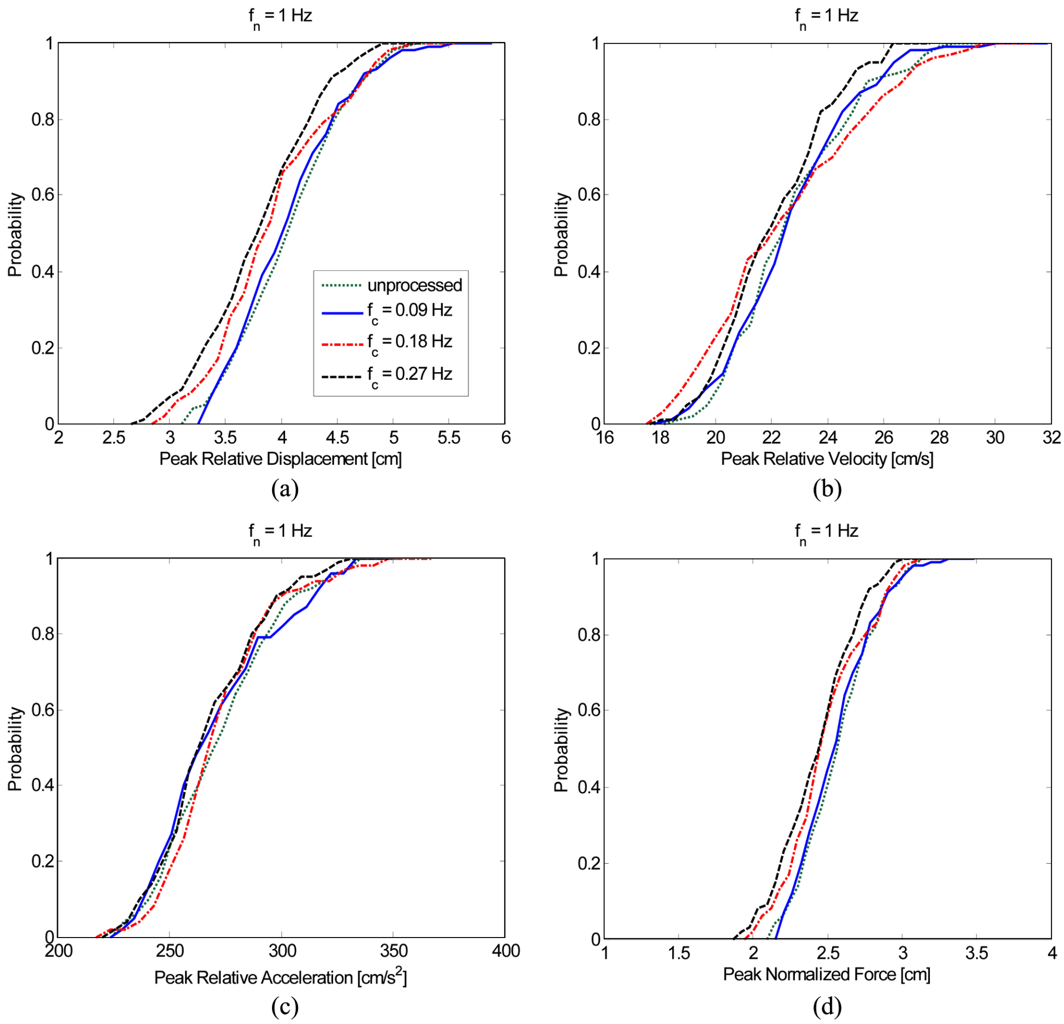

Fig. 10 Cumulative distribution functions of the peak response of a nonlinear single-degree-of-freedom oscillator with natural frequency $f_n = 1$ Hz subjected to sets of 100 ground motion simulations processed with three filter corner frequencies, $f_c = 0.09$ Hz, 0.18 Hz and 0.27 Hz; the oscillator's peak response subjected to a set of 100 unprocessed acceleration simulations is also shown in the figures. Part (a) presents the probability distribution of the oscillator's peak relative displacement, part (b) its peak relative velocity, part (c) its peak relative acceleration and part (d) the peak total spring force normalized with the system's stiffness

system's stiffness.

Fig. 9 indicates that the differences in the stiffer ($f_n = 5$ Hz) system's dynamic response for unprocessed and processed input excitations are statistically insignificant. The lines depicting the CDFs of the response quantities in the figure are intermingled without any recognizable pattern. As anticipated, for the dynamic response of oscillators with a natural frequency far removed from the high-pass filter corner frequency, any of the considered values ($f_c = 0.09$ Hz, 0.18 Hz and 0.27 Hz) is adequate. Further considerations for the selection of the filter corner frequency for such stiff systems based on their pseudo-static response will be elaborated upon in the following subsection. Some

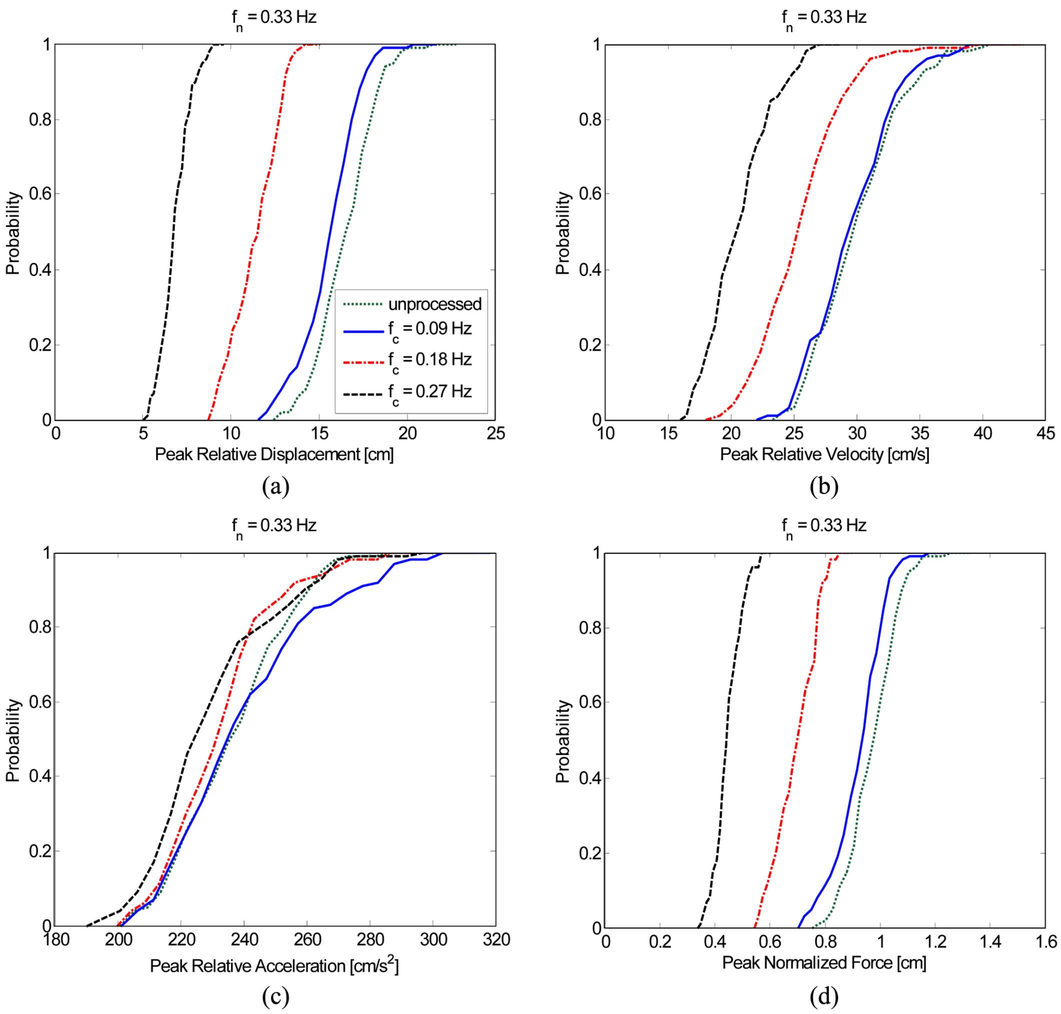

Fig. 11 Cumulative distribution functions of the peak response of a nonlinear single-degree-of-freedom oscillator with natural frequency $f_n = 0.33$ Hz subjected to sets of 100 ground motion simulations processed with three filter corner frequencies, $f_c = 0.09$ Hz, 0.18 Hz and 0.27 Hz; the oscillator's peak response subjected to a set of 100 unprocessed acceleration simulations is also shown in the figures. Part (a) presents the probability distribution of the oscillator's peak relative displacement, part (b) its peak relative velocity, part (c) its peak relative acceleration and part (d) the peak total spring force normalized with the system's stiffness

patterns regarding the effect of processing start becoming recognizable when the system's natural frequency decreases from 5 Hz to 1 Hz, as illustrated in Fig. 10. The CDFs of the peak relative acceleration response (Fig. 10(c)) remain very similar for the unprocessed and processed input excitations, as was the case for the stiffer system (Fig. 9(c)). For the peak relative velocity (Fig. 10(b)), the distribution functions are, again, intermingled, but the unprocessed simulations and the ones processed with $f_c = 0.09$ Hz are in better agreement. The CDFs of the peak relative displacements and normalized forces (Figs. 10(a) and (d), respectively) further confirm the agreement between the unprocessed simulations and the ones processed with $f_c = 0.09$ Hz, suggesting that, for capturing the dynamic response of this more flexible system, a filter corner frequency of 0.09 Hz is more appropriate. A clear indication that the higher high-pass filter corner frequencies reduce the structural response can be noted in Fig. 11, which depicts the statistics of the response of the nonlinear oscillator with a natural frequency of 0.33 Hz. Whereas the CDFs of the peak relative accelerations (Fig. 11(c)) for all processing scenarios do not vary significantly, processing of the simulated time series with the higher corner frequencies (f_c = 0.18 Hz and 0.27 Hz) underestimates considerably the dynamic response in terms of peak relative displacements, velocities and normalized forces (Figs. 11(a), (b) and (d), respectively). Regarding the lower filter corner frequency considered herein (f_c = 0.09 Hz), Fig. 11(b) indicates that it fairly adequately captures the peak relative velocities of the system, but Figs. 11(a) and (d) suggest that it starts underestimating the peak relative displacements and normalized forces of the SDOF oscillator. Clearly, for this flexible system, processing with filter corner frequencies lower than 0.09 Hz is only acceptable.

The aforementioned approach utilized the ASCE 7-10 response spectrum with parameters S_{DS} = 0.5, S_{D1} = 0.2 and T_L = 8 s and a nonlinear system described by the hysteretic softening behavior of the Bouc-Wen model (Wen 1980), as illustrated in Fig. 8. However, the framework for the selection process of the appropriate filter parameters of the processing scheme, so that they capture the dynamic response of lifeline systems, can be reliably extrapolated to any target response spectrum and the linear and any nonlinear structural modeling. As indicated earlier, the evaluation of the filter corner frequency through the analysis of a SDOF oscillator with natural frequency equal to the fundamental frequency of the multi-degree of freedom system suffices for capturing the total dynamic response of the lifeline, as it is the lowest frequency of the structure that will be mostly affected by the high-pass filtering operation.

5.2 Pseudo-static response

The pseudo-static response of lifeline systems is mostly affected by the spatial characteristics of the structure and the ground displacements. Part (c) of Figs. 1 and 3-5 indicate that no processing and various processing approaches can lead to very different displacement waveforms. However, it is not the absolute displacements per se that control the pseudo-static response, but the differential displacements between the supports (Zerva 1992b). Differential ground displacement can be caused by loss of coherency, wave passage and variable site conditions underneath the bridge supports.

Loss of coherency reflects the change in the shape of the waveforms at various ground surface locations. Displacement waveforms, obtained from recorded data at distances pertinent for engineering applications, often show close agreement, as observed, e.g. by Boore *et al.* (2002) from the analysis of data recorded during the 1999 Hector Mine earthquake at a (fairly long) separation distance of 1.6 km. Hence, coherency models that yield spatial correlations tending to unity at low frequencies are more appropriate for engineering applications (Zerva 2009). One of such models is the versatile coherency model of Luco and Wong (1986) given by the expression

$$\gamma(\xi, \omega) = exp[-(\alpha\ \xi\ \omega)^2] \tag{12}$$

in which the coherency drop parameter a is a function of the shear wave velocity and the random properties of the underlying medium. Fig. 12(a) presents the exponential decay of the model with frequency at three separation distances of ξ = 100 m, 300 m and 500 m for an illustrative value of the coherency drop parameter (α = 2.5×10^{-4} s/m). Fig. 12(b) is a "zoom in" of Fig. 12(a) at low frequencies ($f \leq 1$ Hz). It can be seen from Fig. 12(b) that, for the particular coherency model and its coherency drop parameter, motions are essentially fully correlated in the frequency range of $f < 0.3$ Hz, which encompasses the values of the filter corner frequencies utilized herein. However, the high-pass filter reduces the amplitudes of the lower frequency components of the motions over a wider frequency range, as illustrated in Fig. 2(b) and part (d) of Figs. 3-5. Figs. 3(d), 4(d), 5(d) and 12(b) then suggest that the lower values of the filter corner frequencies (e.g. Fig. 3(d)) maintain significant low-frequency ($f \leq 1$ Hz) components in the ground motions, which may be only partially correlated (Fig. 12(b)), whereas for the higher values of the filter corner frequency (e.g. Fig. 5(d)), these low-frequency components are partially eliminated. These differences in the low-frequency content of the processed simulations caused by the selection of the filter corner frequency will affect the differential ground displacements and, hence, the pseudo-static response of the lifelines and need to be taken into consideration. Wave passage implies that the seismic waveform propagates unchanged on the ground surface. Since most spatial variability models have been developed from seismic data recorded during the strong motion shear wave window, appropriate values for the apparent propagation velocity used in the analysis should be higher than the shear wave velocity in the underlying bedrock (Zerva 2009), i.e., generally, of the order of km/s. Clearly, the different waveforms of Figs. 3(d), 4(d) and 5(d) propagating with such velocities on the ground surface will induce different differential motions, and, again, affect the pseudo-static response of the systems. Obviously, variable site conditions underneath the structure's supports (e.g. rock conditions underneath the abutments and soft soil conditions underneath the piers) will induce significant differential ground displacements. This scenario, however, may not be readily simulated via spectral representation due to the possible formation of surface waves in sedimentary valleys (e.g. Zerva and Stephenson 2011).

Since the pseudo-static response depends highly on the spatial characteristics not only of the ground motions but also, those of the structure, the selection criterion for the filter corner frequency cannot be isolated from the unique spatial characteristics of each lifeline system. It is noted that, generally, the relative contribution of the pseudo-static response of the structures to its total response

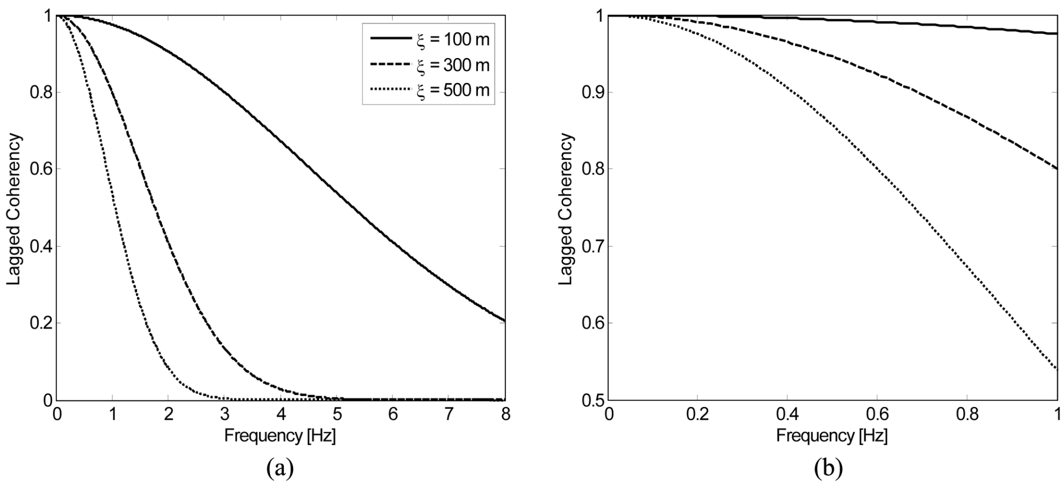

Fig. 12 The variation of the coherency model of Luco and Wong (1986) with frequency at three separation distances of 100 m, 300 m and 500 m in part (a); the coherency drop parameter used in the illustration is $\alpha = 2.5\times10^{-4}$ s/m. Part (b) is the same illustration as part (a) only zoomed in the low frequency range ($f \leq 1$ Hz)

becomes more pronounced as the system becomes stiffer (Zerva 1990). For the more flexible systems of Figs. 10 and 11, one may speculate that the filter corner frequency that sufficiently reproduces the system's dynamic response should suffice for the pseudo-static contribution. However, this speculation may not valid for the stiffer system of Fig. 9, for which the examination of the dynamic response indicated that any value of the filter corner frequency can adequately reproduce the system's dynamic response. A conservative estimate for the filter corner frequency needed to capture the pseudo-static response can then be obtained by analyzing the pseudo-static response of the system subjected to spatially variable excitations processed with the various corner frequencies. It is noted that the displacement waveforms processed with the low filter corner frequency (Fig. 3(c)) have the highest absolute amplitudes but vary more slowly with time due to their richer low-frequency content. On the other hand, the displacement waveforms processed with the higher filter corner frequency (Fig. 5(c)) have significantly lower absolute amplitudes but vary more rapidly with time due to the more considerable elimination of their lowest frequencies. The more severe pseudo-static response resulting from the different processing scenarios will then indicate the appropriate estimate of the filter corner frequency. In this way, the spatial characteristics of both the ground motions and the lifeline system will be taken into consideration, and the effect of the processing scheme on the pseudo-static response quantified.

6. Conclusions

A versatile and quick tool for simulating artificial spatially variable acceleration time series compatible to a prescribed response spectrum for the seismic response evaluation of lifeline systems in a Monte Carlo framework is the spectral representation method. Accelerations thus generated contain artificial, low-frequency components that render the integrated ground velocities and displacements unrealistic. Hence, simulated motions, like recorded data, require processing. However, criteria for the selection of the high-pass corner frequency of the filter in processing recorded data cannot be readily extrapolated to simulated motions. The reason is that there are physical considerations in processing seismic records, i.e., the elimination of low-frequency noise, whereas the low-frequency components of the simulated motions are numerically generated. Hence, for the simulated time series to be appropriately processed, the selection of the filter corner frequency needs to be controlled by the response of the system, for the response evaluation of which the simulated accelerations are generated.

This effort put together an integrated framework for the processing of simulated seismic acceleration time series concentrating on the corner frequency of the high-pass filter. The two-step approach considers both the dynamic and the pseudo-static response of the lifeline system. First, the methodology ensures that the dynamic structural response induced by the processed simulations captures the characteristics of the system's dynamic response caused by the unprocessed simulations, the frequency content of which is fully compatible with the target response spectrum. Second, it further examines the adequacy of the selected estimate for the filter corner frequency by conducting a pseudo-static response evaluation of the system subjected to spatially variable excitations. Clearly, if only the dynamic response of a system is of interest, then the first criterion suffices for the estimation of the appropriate corner frequency of the high-pass filter. The approach sets the bases for the quantitative estimation of the processing scheme to be used in response-spectrum compatible spatially variable seismic time series generated via the spectral representation method or, alternatively, via any other simulation technique that does not provide physical considerations for the selection of the corner frequency of the high pass filter.

Acknowledgments

The first author acknowledges the partial support of the US National Science Foundation under awards CMMI-0600262 and CMMI-0900179. Any opinions, findings and conclusions or recommendations expressed in this material are those of the authors and do not necessarily reflect the views of the US National Science Foundation.

References

American Society of Civil Engineers (2010), *Minimum design loads for buildings and other structures*, ASCE STANDARD, ASCE/SEI 7-10.

Amin, M. and Ang, A.H-S. (1968), "Non-stationary stochastic model of earthquake motion", *J. Eng. Mech.-ASCE*, **94**(2), 559-583.

Akkar, S. and Bommer, J.J. (2006), "Influence of long-period filter cut-off on elastic spectral displacements", *Earthq. Eng. Struct. D.*, **35**(9), 1145-1165.

Boore, D.M. (2011), *Personal Communication*.

Boore, D.M. and Akkar, S. (2003), "Effect of causal and acausal filters on elastic and inelastic response spectra", *Earthq. Eng. Struct. D.*, **32**(11), 1729-1748.

Boore, D.M., Stephens, C. and Joyner, W. (2002), "Comments on baseline correction of digital strong-motion data: examples from the 1999 Hector Mine, California, earthquake", *B. Seismol. Soc. Am.*, **92**(4),1543-1560.

Boore, D.M. and Bommer, J.J. (2005), "Processing of strong-motion accelerograms: Needs, options, and consequences", *Soil Dyn. Earthq. Eng.*, **25**(2), 93-115.

Burdette, N.J., Elnashai, A.S., Lupoi, A. and Sextos, A.G. (2008a) "Effect of asynchronous earthquake motion on complex bridges. I: Methodology and input motion", *J. Bridge Eng.-ASCE*, **13**(2), 158-165.

Burdette, N.J. and Elnashai, A.S. (2008b), "Effect of asynchronous earthquake motion on complex bridges. II: Results and implications on assessment", *J. Bridge Eng.-ASCE*, **13**(2), 166-172.

Comité Européen de Normalisation (CEN) (2005), *EUROCODE 8: Design of structures for earthquake resistance – Part 2: Bridges*, EN 1998-2:2005, Brussels, Belgium.

Converse, A.M. and Brady, A.G. (1992), *BAP-basic strong-motion acceleration processing software*; Version 1.0, Open-File Report 92-296A, US Geological Survey, Denver, Colorado.

Deodatis, G. (1996), "Simulation of ergodic multivariate stochastic processes", *J. Eng. Mech.-ASCE*, **122**(8), 778-787.

FHWA (1996a), *Seismic design of bridges design example No. 1 – Two-span continuous CIP concrete box bridge*, Report No. FHWA-SA-97-006, Federal Highway Administration.

FHWA (1996b), *Seismic design of bridges design example No. 4 – Three-span continuous CIP concrete bridge*, Report No. FHWA-SA-97-009, Federal Highway Administration.

Hao, H., Oliveira, C.S. and Penzien, J. (1989), "Multiple-station ground motion processing and simulation based on SMART-1 array data", *Nucl. Eng. Des.*, **111**(3), 293-310.

Liao, S. and Zerva, A. (2006), "Physically compliant, conditionally simulated spatially variable seismic ground motions for performance based design", *Earthq. Eng. Struct. D.*, **35**(7), 891-919.

Lou, L. and Zerva, A. (2005), "Effects of spatially variable ground motions on the seismic response of a skewed, multi-span bridge", *Soil Dyn. Earthq. Eng.*, **25**(7-10), 729-740.

Lupoi, A., Franchin, P., Pinto, P.E. and Monti, G. (2005), "Seismic design of bridges accounting for spatial variability of ground motion", *Earthq. Eng. Struct. D.*, **34**(4-5), 327-348.

Monti, G., Nuti, C. and Pinto, P.E. (1996), "Nonlinear response of bridges under multi-support excitation", *J.*

Struct. Eng.-ASCE, **122**(10), 1147-1159.

Moustafa, A., Ueno, K. and Takewaki, I. (2010), "Critical earthquake loads for SDOF inelastic structures considering evolution of seismic waves", *Earthq. Struct.*, **1**(2), 147-162.

New York City Department of Transportation (NYCDOT) (1998), *Seismic criteria guidelines*, New York, NY.

Rice, S.O. (1944), "Mathematical analysis of random noise", *Bell Syst. Tech. J.*, **23**(3), 282-332.

Safak, E. and Boore, D.M. (1998), "On low-frequency errors of uniformly modulated filtered white-noise models for ground motions", *Earthq. Eng. Struct. D.*, **16**(3), 381-388.

Saxena, V., Deodatis, G., Shinozuka, M. and Feng, M. (2000), "Development of fragility curves for multi-span reinforced concrete bridges", *Proceedings of the International Conference on Monte Carlo Simulation*, *MCS-2000*, G.I. Schueller and P.D. Spanos editors, Monte Carlo, Monaco.

Shinozuka, M. (1974), "Digital simulation of random processes in engineering mechanics with the aid of FFT technique", in *Stochastic Problems in Mechanics*, S.T. Ariaratnam and H.H.E. Leipholz editors, University of Waterloo Press, Ontario, Canada.

Shinozuka, M. (1971), "Simulation of multivariate and multidimensional random processes", *J. Acoust. Soc. Am.*, **49**(1), 357-367.

Shinozuka, M., Saxena, V. and Deodatis, G. (2001), "Effect of spatial variation of ground motion on highway structures", *Final Technical Report for Tasks 106-E-2.2 to 106-E-2.5*, FHWA Contract DTFH61-92-C-00106, The NCEER Highway Project, Seismic Vulnerability of Existing Highway Construction.

Spanos, P.D., Giaralis, A. and Jie, L. (2009), "Synthesis of accelerograms compatible with the Chinese GB 50011-2001 design spectrum via harmonic wavelets: Artificial and historic records", *Earthq. Eng. Eng. Vib.*, **8**(2), 189-206.

Trifunac, M.D. (1971), "Zero baseline correction of strong-motion accelerograms", *B. Seismol. Soc. Am.*, **61**(5), 1201-1211.

Tzanetos, N., Elnashai, A.S., Hamdan, F.H. and Antoniou, S. (2000), "Inelastic dynamic response of RC bridges subjected to spatially non-synchronous earthquake motion", *Adv. Struct. Eng.*, **3**(3), 191-214.

Wen, Y.K. (1980), "Equivalent linearization for hysteretic systems under random excitation", *J. Appl. Mech.-ASME*, **47**(1), 150-154.

Wong, C.W., Ni, Y.Q. and Ko, J.M. (1994), "Steady-state oscillation of hysteretic differential model. II: Performance analysis", *J. Eng. Mech.-ASCE*, **120**(11), 2299-2325.

Zaré, M. and Bard, P.Y. (2002), "Strong motion dataset of Turkey: Data processing and site classification", *Soil Dyn. Earthq. Eng.*, **22**(8), 703-718.

Zerva, A. (1990), "Response of multi-span beams to spatially incoherent seismic ground motions", *Earthq. Eng. Struct. D.*, **19**(6), 819-832.

Zerva, A. (1992a), "Seismic ground motion simulations from a class of spatial variability models", *Earthq. Eng. Struct. D.*, **21**(4), 351-361.

Zerva, A. (1992b), "Seismic loads predicted by spatial variability models", *Struct. Saf.*, **11**(3-4), 227-243.

Zerva, A. (2009), *Spatial variation of seismic ground motions: Modeling and engineering applications*, CRC Press, Taylor & Francis Group, ISBN 978-0-8493-9929-9.

Zerva, A. and Stephenson, W.R. (2011), "Stochastic characteristics of seismic excitations at a non-uniform (rock and soil) site", *Soil Dyn. Earthq. Eng.*, **31**(9), 1261-1284.

SA